36th AIAA Plasmadynamics and Lasers Conference
6-9 June 2005, Toronto, Canada
AIAA-2005-4772

Shear Layers and Aperture Effects for Aero-Optics

John P Siegenthaler*, Stanislav Gordeyev †, and Eric Jumper‡
Hessert Laboratory, University of Notre Dame, Notre Dame, IN, 46446-5684, USA

This paper examines the effect of a finite aperture on wavefronts, especially with regard to aero-optic distortions from a shear layer. When the net deflection of a beam is corrected in real time to bring a beam on target, a common practice in optic applications even if no other corrections are performed, this removal of the off-target tilt and the finite aperture of the beam act as a spatial filter. This restricts the tip-tilt correction and the wavefront correction to separate frequency ranges, causing the rms magnitude of the remaining distortion to be corrected to vary with aperture size. It has also been found that for a shear layer, aperture size is a key factor in scaling the severity of optical distortions, and it is likely to be a key component in scaling other types of optically-aberrating flows.

1. Nomenclature

a	=	local speed of sound
AO	=	Adaptive Optics
A_p	=	aperture length
C	=	amplitude of oscillation
DM	=	Deformable Mirror
f	=	frequency
f_d	=	dominant frequency at a location
$f_{T/T}$	=	maximum T/T frequency filtered
g,h	=	generic functions
K_{GD}	=	Gladstone-Dale constant, 0.000227 m^3/kg
L	=	length scale
M	=	Mach number
OPD	=	Optical Path Difference
OPD_{rms}	=	root mean square of the OPD over an aperture
OPL	=	Optical Path Length
p	=	pressure
r_u	=	velocity ratio U_2/U_1
s	=	density ratio ρ_2/ρ_1
T	=	temperature
T/T	=	Tip-Tilt
u	=	velocity
$U_{1,2}$	=	sheer layer flow velocities
U_C	=	convection velocity of the shear layer
α_x	=	deflection angle of a beam in the x direction

* Graduate Research Assistant, Aerospace and Mechanical Engineering, Notre Dame, Student Member AIAA
† Assistant Research Professor, Aerospace and Mechanical Engineering, Notre Dame, Member AIAA.
‡ Professor, Aerospace and Mechanical Engineering, Notre Dame, Fellow AIAA.

δ = boundary layer thickness
δ_{vis} = thickness of the shear layer as estimated by flow visualization.
Δt = time step
Δx = spatial distance of flow convection in time Δt
Λ = streamwise length of large structures in the shear layer
ρ = density

2. Introduction

WHEN a laser beam with an otherwise planar wavefront is projected through a variable-index-of-refraction turbulent flow, its wavefront becomes aberrated. To the extent that the wavefront is aberrated across the beam's aperture, the beam's ability to create a high-intensity spot at the target in the far field is hampered.[1] An adaptive-optic (AO) system can be used to measure and then compensate for the aberrations that are to be imprinted on the beam's wavefront by imposing a conjugate wavefront figure on the beam prior to projecting it through the aberrating medium so that in a perfect case the beam emerges unaberrated.[2] In practice the conjugate is imposed in at least two stages. First, the aberration must be measured. Because of the linear nature of optics, the aberration that will be imposed by a beam propagating through the aberrating medium in one direction can be determined by measuring the aberration imposed by an otherwise near-planar wavefront propagated through the medium in the opposite direction. Presumably this would be some sort of return from the target. In the case of a free-space communication system, the target is cooperative and can emit a diverging beam that will arrive at the entrance pupil of the beam director as if it were a pinhole source at the target. The wavefront from this far-field return then enters the adaptive-optic beam train.

One realization of the layout of the adaptive-optic beam train is the Notre Dame adaptive-optic system designed by Xinetics in cooperation with the Albuquerque Boeing, SVS group. A schematic of the system is shown in Fig. 1. What can be noted in Fig. 1 is that the first correction element the incoming beam encounters is a tip-tilt (T/T) mirror; an enlargement of the components of the T/T mirror is shown in Fig. 2. As implemented, this portion of the system makes use of technology that has long been available for maintaining alignment between multiple optical benches and in the present case is, in fact, used to maintain the alignment of the incoming beam into the remaining elements of the system. The enlargement in Fig. 2 shows one of the critical placement considerations of the T/T mirror; the T/T mirror is re-imaged on the deformable mirror (DM) which, in effect, adds an ability of the DM to tip and tilt.

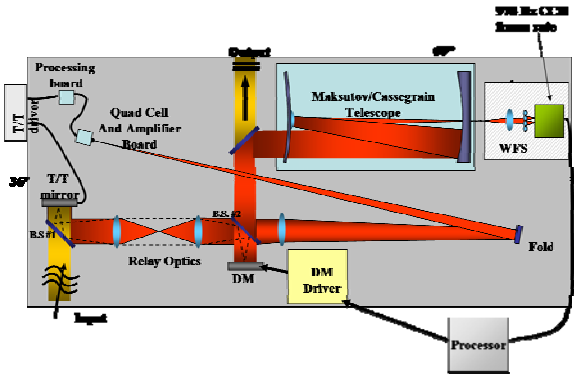

Figure 1. Schematic of Notre Dame Adaptive-Optic System cooperatively developed by Xinetics and Boeing SVS.

Note also that the T/T mirror is controlled by a separate, in this case analog, stand-alone processor. The beam is focused onto a position-sensing device, which in this case is a quad cell. Tip-tilt mirrors can be made to have relatively high bandwidth so that one can presume that the remainder of the AO system need not contend with removing overall tip and tilt. In fact, essentially all modern beam-director systems incorporate T/T mirrors on their optical benches even when no other AO system components are present. It should be noted that we have also incorporated near-stationary correction components into our AO system for some experiments to remove mean aberration.

Because of the ubiquitous use of T/T mirrors, when we make time-resolved wavefront measurements to characterize aero-optic environments, we typically remove both tip and tilt and time-averaged mean aberration leaving only the unsteady component over the

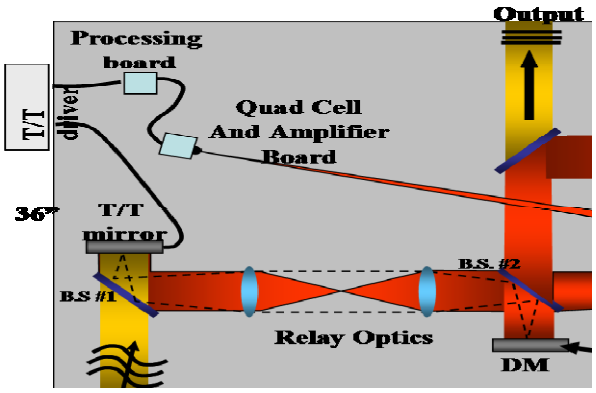

Figure 2. Detail of the Tip-Tilt Compensation portion of the system.

aperture. It is important to note that the aperture itself imposes a spatial filter on the overall aberrating character of the medium. Because the aberrations are due to turbulent flow, which by definition is convecting, this spatial filter is associated with a concomitant temporal frequency. Thus, low frequency aberrations with coherence length Λ, and a convection velocity U_c, will result in low-bandwidth tip and tilt that a T/T mirror will remove. As an aside, this fact allows facilities that might otherwise be presumed to be unacceptable for aero-optic testing to be usable by simply removing tip and tilt from each wavefront frame.

3. Shear Layers

Shear layers, also known as mixing layers, occur at the boundary between two parallel flows of different fluids, or even the same fluid moving at different velocities. The transfer of momentum in the vicinity of the boundary causes this boundary region to grow in size as it convects downstream. Kelvin Helmholtz instability produces ripples in the boundary along its span that also grow and contribute to the growth of the layer region. These perturbations eventually roll up into vortical structures that grow, pair, and merge as the shear layer grows.[3]

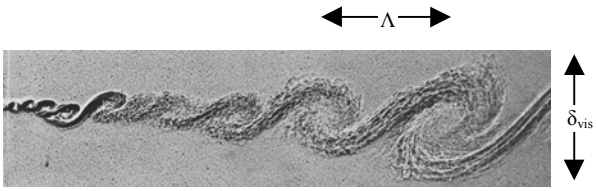

Figure 3. The classic shear layer.
(Konrad, 1976)

When there is a large difference in relative velocity between the two flows, the low pressure well found in the center of these structures, also known as rollers, can be quite pronounced.[4] This drop in pressure is accompanied by a drop in density, with its concomitant change in index of refraction. This makes these structures of interest from an optical standpoint. While there are many elements in a compressible flow of this sort that can produce optical distortions, the low pressure wells associated with these rollers are likely to be the most significant contributor in that regard.

Shear layers grow linearly in thickness with distance from their starting point. There are multiple definitions for the thickness of a shear layer, such as momentum thickness and vorticity thickness, and the growth rate of the shear layer is less well understood for compressible flows than for incompressible and weakly-compressible shear layers.. In these experiments, the primary method for estimating the layer thickness was by visual observation of the vortical structures in the flow. The literature[5] reports that this vorticity thickness (δ_{vis}) can be estimated from the following empirical relation:

$$\frac{d\delta_{vis}}{dx} \approx 0.17 \frac{(1-r_u)(1+\sqrt{s})}{1+r_u\sqrt{s}}, \tag{1}$$

where r_u is velocity ratio (U_2 / U_1) and s is the density ratio (ρ_2 / ρ_1) of the two flows making up the shear layer.

For this optical study, the dimension in the layer of primary interest is not the thickness, but the spacing between rollers. (Λ) This coherence length is related to δ_{vis} by yet another empirical constant. The literature reports that this ratio of Λ/δ_{vis}, varies from 1.5 (Ref 6) to 2 (Ref 7). In observing a flow passing a point of measurement, the average length of a repeating structure can be found by the relationship

$$\Lambda = \frac{U_C}{f_d} \tag{2}$$

where f_d is the frequency or average frequency at which the structure is seen to pass by the point of measurement. It should be noted that Λ differs from Λ_n reported in Ref 8, where the frequency in Eq. (2) is replaced with f_n. That frequency is biased towards larger structures by the fact that the larger structures produce a larger-amplitude optical response.

4. Small Beam Aero-Optic Measurements

Optical distortions can be thought of in terms of deflection angles for isolated rays of light, or as wavefronts. A wavefront is a sheet of light, with the same wavelength and phase throughout. A planar wavefront is a flat sheet of this sort, and models what one might expect in a collimated laser beam of some non-zero aperture (A_p). A

wavefront is a more complete expression of the optical effects of a flow, as a wavefront is composed of all the rays passing through the flow from that direction or source.

While a wavefront contains all the relevant aspects of the light and distortions to the light passing through an aberrating flow or medium, there is such a thing as having too much information. Interferometry and phase diversity can measure a wavefront in its entirely, and some other types of sensors can be built with impressive spatial resolution. However, for many applications, far less information is better. For real-time applications dealing with a time-varying system, there is often a trade-off between how rapidly one can sample and process data and the amount of data one can sample. The data in this paper was acquired with a Malley probe,[10] which uses two beams that are narrow, relative to the length scale of structures in the flow, and so are deflected as rays rather than distorted as wavefronts. A detailed description of the components and reconstruction methods for optical wavefronts using a Malley probe can be found in Ref 10.

By definition a wavefront is a locus of points of constant phase.[11] As shown in Fig. 4, as an initially planar wavefront for a collimated laser beam propagates through a region of variable index of refraction, portions of the wavefront become advanced and retarded from the wavefronts mean position. If a plane is drawn normal to the wavefront's mean propagation direction, the beam's phase along that plane will be greater or less than the phase of the wavefront at the mean position. It is the phase difference over this plane that is referred to as the beam's aberration. According to Huygens' principle the wavefront can be replaced by pinhole sources along its surface, each emitting spherical waves and the wavefront can be redrawn at some distance by connecting surfaces of constant phase from the pinhole sources.[11] This leads to the result that wavefronts propagate normal to themselves and is the basis for geometric optics. As a consequence, a ray, everywhere perpendicular to the wavefront can be traced along the wavefronts propagation path as shown in Fig. 4. The angle at which the ray emerges from the aberrating medium, being normal to the emerging wavefront will have an off-axis angle, shown as $-\alpha_x$ in Fig.4, which is equal to the wavefront's x-gradient.

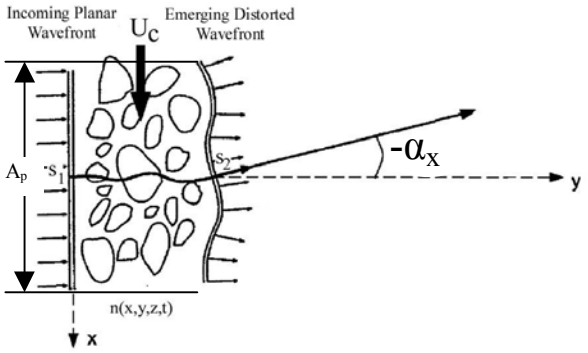

Figure 4. An optical ray as part of a wavefront through a distorting flow field.

Hartmann was the first to realize that this fact could be used to measure the figure of wavefronts.[12] He placed an opaque, perforated plate in front of the aberrated wavefront with a photographic plate at a known distance from the perforated plate. By exposing the photographic plate first to an unaberrated beam and then to the aberrated beam he was able to measure the off-axis displacement of beams emerging from the perforations. Knowing the distance between the plates he could determine the angles and thus the wavefront slopes at each perforation (measurement location) and then through integration determine the wavefront's aberrated figure. Similar measurements can be made by passing small-aperture beams through the aberrating medium.

Malley et. al. were the first to recognize that when the aberrating medium is a turbulent flow, the aberrations caused by the convecting flow structures will, convect as well.[9] Thus, a single beam propagated through the flow could be used to measure a continuous time series of wavefront slopes as the wavefront convects by the measurement location. The Malley principle has been used at Notre Dame to develop a series of wavefront-measurement devices.[13,14,15] To the extent that the flow can be treated as slowly varying, the Taylor frozen flow assumption can be used to compute wavefronts up and downstream of the measurement location, which are reasonably accurate for some distance up and downstream. By propagating two small-aperture, closely-spaced, beams through the flow, both the wavefronts slope and its convection speed can be determined.

$$\frac{dOPL(t)}{dx} = -\alpha_x(t) \tag{3}$$

In order to integrate the slope to produce a running time series of OPL(t), the velocity is required as

$$OPL(t) = \int \frac{dOPL(t)}{dx} dx = \int \frac{dOPL(t)}{dx} U_c dt \tag{4}$$

where $U_c = dx/dt$. By knowing the distance between beams and cross-correlating the beams to find the delay time between the two beams' signals, U_c can be determined,[10] so that

$$OPL_x(t) = \int_{t_0}^{t} -\alpha_x(\tau) U_c d\tau \tag{5}$$

From these equations and relationships, an approximation of the OPL over a portion of the flow can be reconstructed from spatially coarse data, or even a single point of measurement. An important aspect of wavefronts that becomes apparent in this form of reconstruction is the relationship between length scale of the aberrations and the amplitude of the resulting OPD. If α_x were a pure sine wave, then the OPL would be

$$OPL_x(t) = \int_{t_0}^{t} -C\sin(2\pi f\tau) U_c d\tau = U_C \frac{C}{2\pi f}\cos(2\pi f(t - t_0)) \tag{6}$$

By Eqs. (2) and (6), the amplitude of OPLs associated with deflection data of a given amplitude will be inversely proportionate to the frequency of that deflection and directly proportional to the length of the structures.

The OPL produced by Eq. (5) can be made to any length by setting the upper and lower bounds of the integral. However, the measurement technique is only valid if the frozen flow assumption is valid, and that is only true for regions close to the points where the beam passes through the flow. As one extrapolates an OPL further upstream or downstream from a location of measurement, the data becomes less valid with increasing distance from that point.

5. Aperture Effects

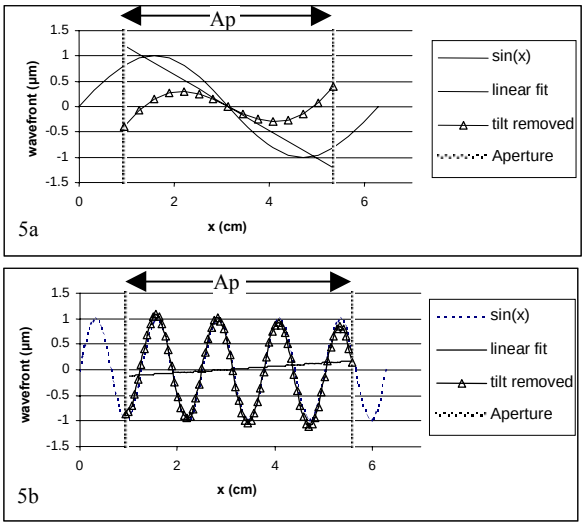

Figure 5. Examples of the spatial filter effect produced by an aperture and tip-tilt removal.

While this technique of reconstruction and estimation is only accurate over short distances, real-world applications involve beams of a finite diameter, and measurements relating to these applications only need to be accurate over that area. The finite aperture also has an effect on those structures in the flow that will produce distortions within the boundaries of the beam's wavefront over the aperture that will deflect or tilt the beam as a whole.

Figure 5 shows two wavefronts, both aberrated into the form of a sine wave, with the same amplitude, over the same length of aperture. In Fig. 5a, the period of the wave is a bit longer than the aperture. A linear fit to this wavefront over the aperture shows a significant degree of net tilt, which, as discussed earlier, would deflect the beam. Removing this tilt to place the beam on target also reduces the amplitude of the variations in the wavefront in this case by more than 50%. Figure 5b shows the effects of T/T removal when the spatial scale of the distortions is smaller than the aperture. In that case, there is very little net tilt and tilt removal has little effect on the magnitude of the aberration.

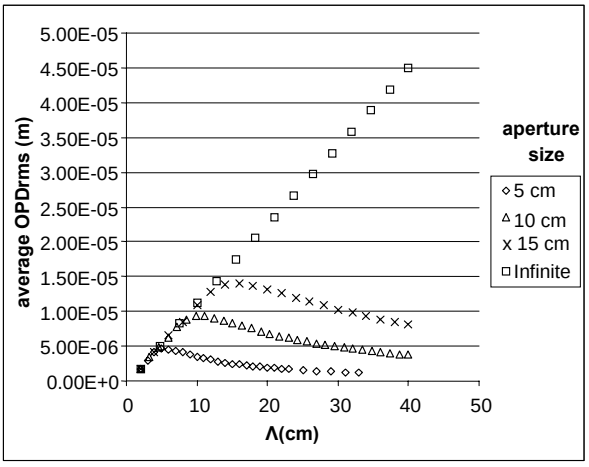

Figure 6. Results for simulated α=sin(ωt)

A finite aperture of a physical beam acts as a spatial filter, separating the distortions caused by larger-scale structures from those caused by smaller-scale structures. If $A_p/\Lambda << 1$, then T/T deflection becomes the only significant effect of distortions on that length scale. This would seem to indicate that the most severe wavefront distortions come from distorting structures in the flow that are smaller than the aperture. However, there is a countervailing effect seen in the wavefront reconstruction algorithms and formulas that produces OPD variations of greater amplitude for aberrations of the largest length scales. This is addressed in Eq. (6) and the associated text.

Figure 6 was generated by using a pure sine function of extended coherence length as the beam deflection, α. Each point is the time averaged rms OPD (OPD_{rms}) for a fixed period of α and a fixed A_p. Each set of points shares a common value for A_p while Λ varies. For an infinite aperture, the average OPD_{rms} grows linearly with Λ, as indicated by Eq. (6). For a finite aperture, this is true only for $\Lambda < A_p$. For $\Lambda > A_p$, OPD_{rms} tapers off asymptotically as Λ increases.

This filter effect can also be found and expressed analytically. For a wavefront or other input of the form g(x,t), OPD_{rms}, as a function of time over an aperture with T/T removal, will be:

$$OPD_{rms}\left(A_p,t\right)=\sqrt{\int_0^{Ap}\left[g(x,t)-\left(A(t)+xB(t)\right)\right]^2 dx} \tag{7}$$

where A and B in Eq. (7) are the coefficients of a linear fit to the overall tilt and piston present in g(x,t). It just so happens that finding values for A and B to minimize the function inside the square root in Eq. (7) is the basis for performing such a linear fit, which explains why T/T removal tends to reduce the magnitude of aberrations.

If g(x,t) is set to a sine function:

$$g(x,t)=\sin\left[2\pi f\left(t-\frac{x}{U_C}\right)\right] \tag{8}$$

and the resulting OPD_{rms} is averaged over time, then that average can be compared to the OPD_{rms} for an infinite aperture with no T/T removal. This ratio can be considered the gain of the spatial filter for that length in the distorting structures,

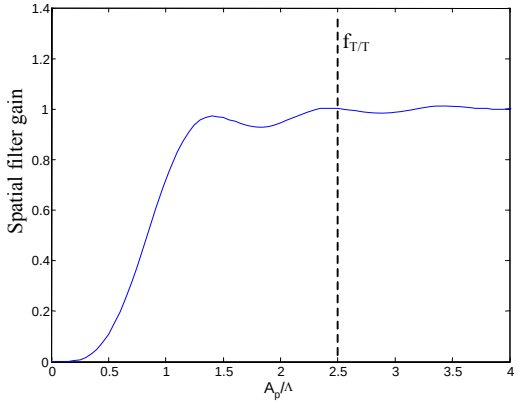

Figure 7. Spatial filter normalized frequency response

$$G(A_p)=\frac{\overline{OPD_{rms}}(A_p)}{\overline{OPD_{rms}}(A_p=\infty)} \tag{9}$$

Figure 7 shows the frequency response of this spatial filter in terms of a nondimensional frequency, A_p/Λ. As can be seen in the Fig. 7, this is a high-pass filter, screening out aberrations with a length scale larger than the aperture. This filter gain can be found analytically from Eq. (7) for a sine signal given in Eq (8), and has the form

$$G\left(\frac{A_p}{\Lambda}\right)=\frac{-3-\pi^2\left(\frac{A_p}{\Lambda}\right)^2+\pi^4\left(\frac{A_p}{\Lambda}\right)^4+\left(3-2\pi^2\left(\frac{A_p}{\Lambda}\right)^2\right)\cos^2\left(\pi\frac{A_p}{\Lambda}\right)+6\pi\frac{A_p}{\Lambda}\sin\left(\pi\frac{A_p}{\Lambda}\right)\cos\left(\pi\frac{A_p}{\Lambda}\right)}{\pi^4\left(\frac{A_p}{\Lambda}\right)^4} \tag{10}$$

This filtration effect has special relevance for shear layers. Two of the defining characteristics of shear layers are the presence of coherent structures in the layer, and that the layer and structures grow linearly as they progress

downstream. Therefore, one would expect the optical distortions to have a characteristic frequency and length scale at each point in the flow, and for that length scale to grow linearly with position downstream in the shear layer.

This also has significance for the engineering of T/T removal systems. The bandwidth required for this system corresponds to the frequencies removed by this filter function. Looking at Fig. 7, this corresponds to frequencies lower than $A_p/\Lambda = 2.5$. Let us call this frequency $f_{T/T}$. By Eq. (2)

$$f_{T/T} = 2.5\frac{U_C}{A_p} \tag{11}$$

The results in Fig. 6 show a similarity in the curves traced for differing values of A_p, with both the maximum value for OPD_{rms} and the value of Λ at which that maximum is seen having a linear relationship with A_p. Both OPD and structure size are in units of length, as is the aperture, so it makes sense to non-dimensionalize those values by A_p. Fig. 8 shows that this causes all the curves to collapse onto one curve.

This result is promising, as scaling laws are valuable tools in applying laboratory results to field applications, but flows that produce optical distortions in the form of a perfect sinewave are hard to come by in the physical world. On the other hand, suggestions of this scaling, and a rules of scaling aero-optics problems in general, can be found from basic theory.

The preceding text defined OPL in terms of the deflection angles often measured and used to reconstruct OPL. The more proper definition of OPL is the integral of the index of refraction along a beam's path, which for air is a function of density.

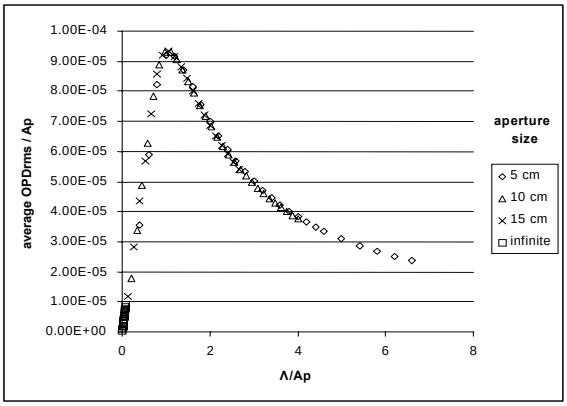

Figure 8. Non-dimensionalized results for α=sin(2πft)

$$OPL(x) = \int 1 + n'(x)ds = \int \left(1 + K_{GD}\left(\rho - \rho_0\right)\right)ds \tag{12}$$

From here it follows that the magnitude of variation in the OPL, which is OPD, will be proportional to the integral of density variations through the flow field. For isentropic flows, changes in density are proportional to changes in pressure and inversely proportional to changes in temperature. The pressure drop inside a vortical structure, such as the ones seen in shear layers, is approximately proportional to the square of their characteristic velocity. Thus, one can find an extending chain of equalities and proportionality,

$$\frac{\Delta\rho}{\rho_0} = \frac{1}{\gamma}\frac{\Delta p}{p_0} \propto \frac{1}{\gamma}\frac{\rho_0}{p_0}U_C{}^2 = \frac{1}{\gamma}\frac{U_C{}^2}{RT_0} = M_C{}^2 \tag{13}$$

where $U_C = (U2\text{-}U_1)/2$ and is the characteristic velocity of the structures, a is the local speed of sound, and M_C is a convective Mach number. OPD, as noted above, is proportional to an integral of $\Delta\rho$, which in turn will be proportional to the magnitude of that variance and the length over which that variance is integrated. In Eq. (1), the diameter of the rollers was chosen as the definition of layer thickness for the shear layer. Thus,

$$OPD_{rms} \propto K_{GD}\Delta\rho\delta_{vis} \propto K_{GD}\rho_0 M_C{}^2\delta_{vis} \tag{14}$$

From Eq. (1), δ_{vis} is proportional to x and Λ is proportional to δ_{vis}.

$$OPD_{rms} \propto \rho_0 M_C^2\Lambda \propto \rho_0 M_C^2 x \tag{15}$$

Thus, the OPD_{rms} tends to grow linearly with Λ, as was the case with the model problem in Eq. (6) and the infinite aperture case in Fig. 6. If flow conditions are fixed, meaning M_C and ρ are constants, then Λ is simply proportional to x. Thus, the shear layer has a characteristic structure size, Λ, that is linearly growing with position, and thus scaling x by A_p should proportionately scale Λ. If the finite aperture and T/T removal truly act as a filter does over all frequencies, regardless of the mix of those frequencies in the input, then all the salient point in the sine function test that make the scaling work should be present in a physical shear layer and optical system. Thus, for fixed flow conditions, there is reason to hope that

$$\frac{OPDrms(x, Ap)}{A_p} = f\left(\frac{x}{A_p}\right) \tag{16}$$

It is left now to examine some actual optical data to see if this does apply.

6. Experimental Setup

The experiments for this study were performed using the Notre Dame Weakly-Compressible Shear Layer (WCSL) facility, shown in Fig 8, located in Notre Dame's Hessert Laboratory for Aerospace Research.

The WCSL facility consists of an inlet nozzle and test section mated with one of Notre Dame's three transonic in-draft, wind-tunnel diffusers. The diffuser section is attached to a large, gated plenum. The plenum is, in turn,

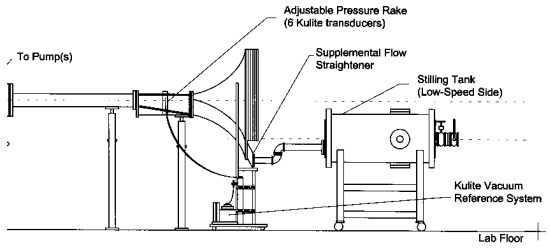

Figure 8. Notre Dame Weakly-Compressible Shear layer facility

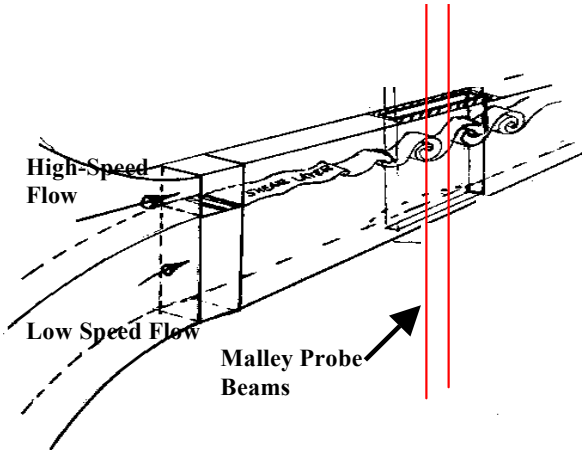

Figure 9. Malley probe positioning

connected to three Allis Chalmer 3,310 CFM vacuum pumps through a sonic throat to prevent unsteady effects from propagating upstream from the pumps. Depending on the gate-valve arrangements, each of these pumps can be used to power separate diffusers, or they can be used in combination to power a single diffuser.

Being an in-draft tunnel, the feeding source is the room total pressure and temperature. The test section is fed from a 104-to-1 inlet nozzle directly from room total pressure on the high-speed side. On the low-speed side, room-total-pressure air is first passed through a settling tank with a "quiet valve" consisting of a bundle of pipes that the flow is forced to pass through at high speed. This produces a loss in total pressure, while keeping its total temperature the same as that of the room air drawn into the high-speed side.

In this set of experiments a Malley probe[10] was used to assess the optical aberrations. In the present case, the Malley Probe's two laser beams were directed through the test section from below, as shown in Fig. 9. All data was filtered to prevent aliasing and to remove low-frequency effects of tunnel vibrations.

7. Physical Results

The data presented here is for the shear layer running with Mach-number values of 0.77 and 0.06 for the high-speed and low-speed flows, respectively. At the pressure and temperature conditions in the test section this translates to velocities of approximately 260 m/s and 35 m/s, with a convection velocity for the shear layer between them of 148 m/s. By Eq. (1), this indicates a δ_{vis} growth rate of approximately 0.25. The predicted growth rate for Λ ranges from 0.375 to 0.5, depending on which recommendation for this relationship is used.[6,7]

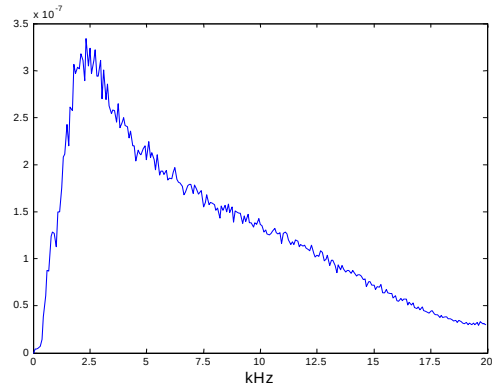

Figure 10. Power density spectrum for deflection data recorded at 13.4 cm.

Unlike the theoretical case explored in section 5, this physical shear layer does not produce optical aberrations in the form of a pure sine function. However, as can be seen in Fig. 10, there is a peak, albeit broad, seen in the power density spectrum of the beam deflection data, indicating at least some periodicity in the data. This peak moves to lower frequencies as the measurement location is moved downstream. For this study, the characteristic frequency was chosen as the frequency at which this peak reaches its maximum value, as this corresponds most closely to the methods and definitions associated with δ_{vis}.[7] As mentioned earlier, other optical studies use a weighted average of this spectrum.[8]

Figure 11 shows the peak frequency of optical disturbances in the shear layer as a function of position downstream from the origin of the shear layer. Figure 12 shows the structure length estimated from the frequencies in Fig. 11 and Eq (2). The trend does appear linear, which is consistent with the arguments leading to the scaling relation of Eq. (16). The line in Fig. 12 represents a value of 2 for Λ/δ_{vis}, which is the maximum value for this ratio found in the literature referenced earlier.[7]

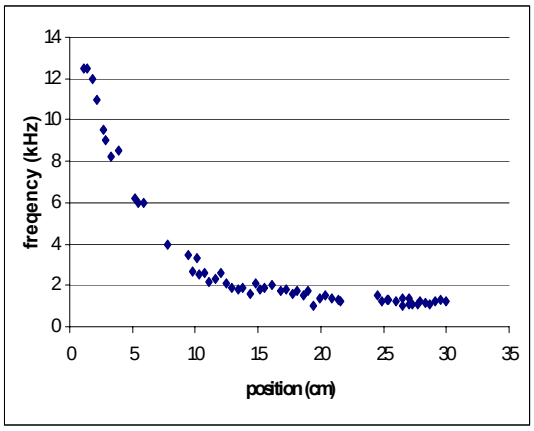

Figure 11. Peak deflection frequencies

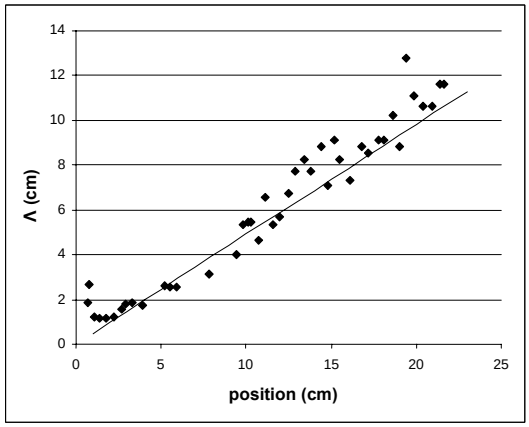

Figure 12. Characteristic Λ and growth rate.

Figure 13 shows the time averaged OPD_{rms} (T/T removed) at a set of measurement locations. Each set of points in this figure represents the OPD_{rms} as calculated for a different size of aperture. Smaller apertures filter out longer wavelengths, and so have lower values of OPD_{rms} in the figure. An aperture of 300 cm can effectively be considered an infinite aperture, and for that aperture size, OPD_{rms} grows almost linearly with position, as it did in

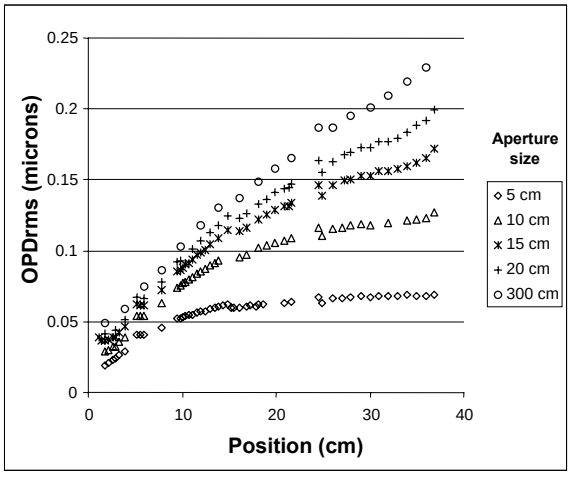

Figure 13. Apertured OPD

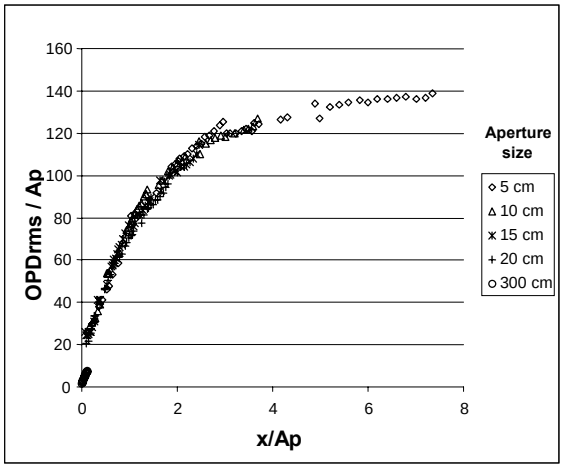

Figure 14 Non-dimensionalized OPD

the simplified test shown in Fig. 6. Also note that from Fig. 12, Λ reaches 5 cm in length at a position somewhere around 11 cm, and in Fig. 13, the curve made up of OPD_{rms} values generated with a 5 cm aperture begins to level off at about that point.

From the results shown in Fig. 6 one might expect the curves to fall off at downstream positions where the characteristic structure length seen in Fig 12 is larger than the aperture. However, as can be seen in the power density spectrum for the data in Fig. 10, the data includes high frequency deflections as well as the lower frequencies associated with the pressure wells in the rollers. This may be caused by smaller irregularities and vortices that roll up into the larger structures; however, it is more likely that it is due to the boundary layer forming between the upper surface of the test section and the high speed flow. The spatial filter of the aperture does not remove these smaller scale optical distortions.

Figure 14 shows that despite these differences, the same practice of non-dimensionalization shown in Figs. 6 and 8 and Eq. (16) applies to the experimental data.

That the scaling law holds true for the experimental results indirectly suggests that the filter function shown in Fig. 7 and Eq. (10) also holds true, but a more direct demonstration can be made. There are difficulties in generating a power spectral density function for apertured OPDs from Malley probe data, as there are few points in the aperture to work with. However, it is possible to generate an apertured OPD for each time step of the recorded data, record the slope of the tilt removed, and generate a psd of that tilt. If the T/T removal does indeed filter out frequencies from the OPD, then the dominant frequencies of the tilt should be the ones removed by that filter. Figure 15 shows the T/T PSD based on the data for the PSD in Fig. 10 and a 5 cm aperture. For U_C = 148 m/s and by Eq. (2), a structure 5 cm in length corresponds to a frequency of about 3 kHz. Fig 15. also shows the inverse of the filter, $(1\text{-}G(A_p/\Lambda))$, scaled by 10^{-7} to fit in the graph vertically and for $A_p/\Lambda = A_p f/U_C = f/3000$ Hz. The exact shape does not and could not be expected to match, since the signal to be filtered does not have a uniform frequency distribution; however, they are high and low in the proper corresponding places. This also verifies Eq. (11), as $f_{T/T}$ for this flow would be 7.5 kHz, which would indeed fulfill the spectrum requirements of the T/T removal. In fact, a bandwidth of 4 kHz on the part of the T/T mirror might suffice.

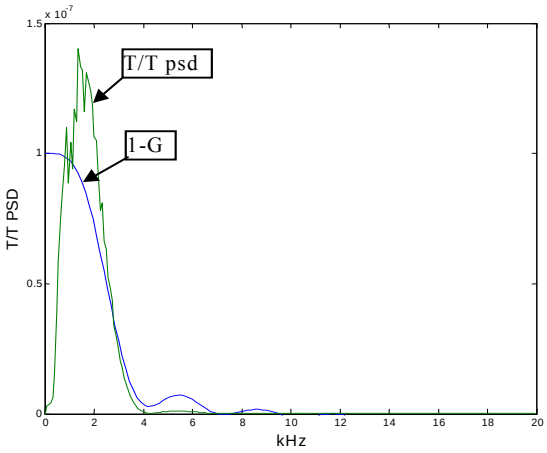

Figure 15. T/T power spectrum and inverse filter

8. Conclusions

This paper has examined the effect of removing tip-tilt over an aperture from aberrated wavefronts. As is now common knowledge, the largest source of aberration for a flow over beam directors on airborne optical systems is when the optical signal passes through a separated shear layer. Under the influences of the Kelvin-Helmholtz instability, shear layers are known to be self-similar. This leads to the formation of linearly-growing, coherent structures that generate optical aberrations that are sinuous in both time and space in the streamwise direction. The results reported here have shown that tilt removal over an aperture acts as a well-defined spatial filter when applied to a sinusoidal train of wavefronts passing through the aperture.

Experimental data obtained for optical propagation through a Mach 0.77 shear layer have been shown to react in an uncannily-similar fashion to the sinusoidal model wavefronts studied here. The linear growth seen in the average structures in shear layers allowed for the juxtaposition of downstream distance from the shear layer's origin and structure size as related to the filter function.

This similarity has revealed some interesting conclusions about the character of aberating structures in shear layers, and in other aberrating flows as well. For example, The relationship between the shear layer's growth in OPD_{rms} and the serendipitous choice of a constant amplitude in the sinusoidal model has suggested avenues for simplified models of a shear layer's optical response. More importantly from operational considerations, this effort has provided an objective approach to determining bandwidth requirements for T/T mirrors for airborne optical systems.

9. Acknowledgments

These efforts were sponsored by the Air Force Office of Scientific Research, Air Force Material Command, USAF, under Grant Number F49620-03-1-0019. The U.S. government is authorized to reproduce and distribute reprints for governmental purposes notwithstanding any copyright notation thereon.

10. References

[1]Jumper, E., and Fitzgerald, E., "Recent Advances in Aero-Optics," *Progress in Aerospace Sciences*, Vol. 37, 2001, pp 299-339.

[2]Tyson, R.K., Principles of Adaptive Optics, Academic Press, Inc, San Diego, 1991.

[3]Ho, C-M, and Huerre, P., "Perturbed Free Shear Layers," *Annual Reviews of Fluid Mechanics*, **16**, 1984, pp. 365-424.

[4]Fitzgerald, E.J., and Jumper E.J., "The Optical Distortion Mechanism in a Nearly Incompressible Free Shear Layer," *Journal of Fluid Mechanics*, Vol. 512, 2004, pp. 153-189.

[5]Papamoschou, D., and Roshko, A., "The Compressible Turbulent Shear Layer: An Experimental Study," *Journal of fluid Mechanics*, Vol. 197, 1988, pp. 453-477.

[6]Brown, G.L., and Roshko, A., "On Density Effects and Large Structure in Turbulent Mixing layers," *Journal of Fluid Mechanics*, Vol 64, No. 4, 1974, pp. 775-816.

[7]Dimotakis, P.E., "Two-Dimensional Shear Layer Entrainment," *AIAA Journal*, Vol. 24, No.11, 1986, pp. 1791-196.

[8]Nightingale, A.M., Gordeyev, S, Jumper, E.J., et. al., "Regularizing Shear Layer for Adaptive Optics control Applications" AIAA Paper 2005-4774, Toronto, Canada, 6-9 June, 2005.

[9]Malley, M., Sutton, G.W., and Kincheloe, N., "Beam-Jitter Measurements for Turbulent Aero-Optical Path Differences," *Applied Optics*, **31,** 1992, pp. 4440-4443.

[10]Gordeyev, S., Jumper, E. J., Ng, T., and Cain, A., "Aero-Optical Characteristics of Compressible, Subsonic Turbulent Boundary Layer." AIAA Paper 2002-3606, Orlando, Florida, 23-26 June, 2003.

[11]Klein M. *Optics*. Wiley, New York, 1970.

[12]Malacara D., Optical shop testing, Wiley, New York, 1978.

[13]Jumper, E. J., and Hugo, R. J., "Quantification of Aero-Optical Phase Distortion Using the Small-Aperture Beam Technique." *AIAA Journal,* **33**(11), 1995, pp. 2151-2157.

[14]Hugo, R., and Jumper, E., "Experimental Measurement of a Time -Varying Optical Path Difference by the Small-Aperture Beam Technique". *Applied Optics*, Vol. 35(22) , 1996, pp. 4436-4447.

[15]Fitzgerald, E.J., and Jumper, E.J., "Two-Dimensional Optical Wavefront Measurements Using as Small-Aperture Beam Technique Derivative Instrument," *Optical Engineering*, Vol. 39, No. 12, Dec. 2000, pp. 3285-3293.